

Aperiodic bursting dynamics of active rotors

Jyoti Sharma, Ishant Tiwari, and P. Parmananda

Department of Physics, Indian Institute of Technology–Bombay, Powai, Mumbai, Maharashtra 400076, India

M. Rivera

Centro de Investigación en Ciencias-(IICBA), UAEM, Avenida Universidad 1001, 62209 Cuernavaca, Morelos, Mexico

(Received 1 October 2021; accepted 10 January 2022; published 27 January 2022)

We report experiments on an active camphor rotor. A camphor rotor is prepared by infusing camphor on a regular rectangular paper strip. It performs self-propelled motion at the air-water interface due to Marangoni driven forces. After some transient (periodic) dynamics, the rotor enters into the aperiodic bursting regime, which is characterized as an irregularly repeated rest (halt) and run (motion) of the rotor. Subsequently, this aperiodic (irregular) rotor is entrained to a periodic (regular) regime with the help of a suitable external periodic forcing. Furthermore, we conducted experiments on two such coupled aperiodic camphor rotors. In this set of experiments, synchronized bursting was observed. During this bursting motion, one rotor follows the movement of the other rotor. A numerical point particle model, incorporating excitable underlying equations, successfully replicated experimentally observed aperiodic bursting.

DOI: [10.1103/PhysRevE.105.014216](https://doi.org/10.1103/PhysRevE.105.014216)**I. INTRODUCTION**

An oscillator can show periodic, aperiodic, or chaotic dynamics [1]. The dynamics of an oscillator are termed aperiodic when at least one of the system variables oscillates with an irregular period. Aperiodic dynamics can be achieved directly after some transients, or the system can display a transition from periodic to aperiodic dynamics [2,3]. Aperiodic dynamics have been observed in a plethora of systems including chemical [4–6], physical [7], and biological [8] systems. Many aperiodic systems show a key behavior known as spiking or relaxation oscillations [9]. In this type of oscillation, one of the system variables displays an excitation or burst followed by a relaxation. These bursts may be periodic or aperiodic. Irregular relaxation oscillations have gained much attention and have been explored in diverse natural and artificial settings [10–12]. An example germane to irregular spiking behavior appears in biological activities such as the EEG (electroencephalogram) and, in some cases, even in an ECG (electrocardiogram). A control of such aperiodic or chaotic dynamics is important because of its relevance to therapeutic treatments [13,14]. Aperiodic dynamics can be morphed into periodic dynamics with the help of an external periodic forcing [15–17], nonfeedback control [18], and even a time delay [19]. The modification of system dynamics using an external forcing typically leads to entrainment of the dynamics, wherein the oscillator phase is mode locked with the phase of the forcing.

In this work, we report experiments showing aperiodic bursting dynamics of an active camphor rotor. The term “active” implies that the rotor moves on the fluidic surface by itself and does not require any external source for motility. In our experiments, rotor is a rectangular strip of paper which

is camphor infused. This rectangular strip can exhibit translational as well as rotational motion at the air-water interface. For this work, we pin this paper strip at one end to curb the translational motion. The strip is thus confined only to perform rotational self-motion at the air-water interface. The motion is evoked by the surface tension imbalance introduced by the inhomogeneously distributed camphor layer around the rotor.

Self-propelled motion of camphor and its derivatives has been extensively reported in experimental as well as numerical studies [20–24]. Reference [25] and Ref. [26] provide a good review in regards to the development of the camphor system. This tabletop experimental system has been used to study complex biological processes as well. For instance, Biswas *et al.* have employed a camphor disk to study first passage time [27] and Tiwari *et al.* have studied a camphor disk string in the context of flagella and cilia motion [28]. Recently, a camphor rotor has been used as a miniature electricity generator [29]. Moreover, a camphor particle has also been realized as a logic gate for information processing [30].

Our previous studies related to the self-propelled camphor rotors have focused on establishing collective dynamics such as synchronization [31,32] and chimeralike states [33] in the periodic domain. In the context of nonlinear aspects of self-propelled entities, efforts have been made to study the relaxation or intermittent dynamics. Notable work in this direction has been reported by Nakatas’ group [34,35]. The intermittency was achieved by pouring surfactant at the air-water interface [36,37] or by increasing the number of camphor disks [35] or by changing the camphor disk position on the attached plastic sheet [38]. However, most of these studies focus on circular particles. To the best of our knowledge, there has not been any experimental proof of

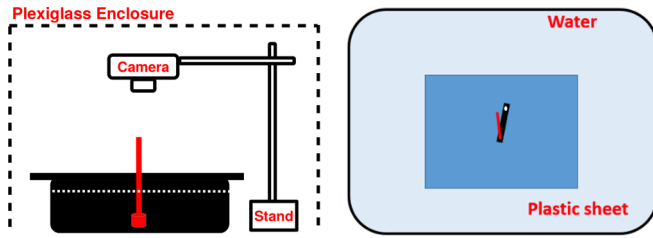


FIG. 1. Schematic diagram of side (left) and camera (right) view of experimental setup. The red color solid line represents the needle used for making the pivot. The white dashed line imitates the plastic sheet placed on the water surface. The setup is the same for all experiments, except a miniature air pump was positioned outside the container for entrainment experiments and the number of pivots was two for the synchronization experiments.

aperiodicity in the active rotors placed at the air-water interface. Towards this end, we performed experiments on such a self-propelled camphor rotor.

In the present work, three sets of experiments were conducted. First, we showed the presence of aperiodic bursting dynamics in a single pinned camphor rotor. “Bursting” here refers to the rotor’s halt (stop) and go (motion). Throughout the manuscript, an irregular repetition of this bursting is called “aperiodic dynamics or aperiodic bursting dynamics” of the camphor rotor. Next, control experiments were performed: wherein a rotor was subjected to an external periodic signal. This forcing resulted in the entrainment of the rotor to the perturbation frequency and, consequently, displaying periodic bursting dynamics. Lastly, we studied a pair of coupled aperiodic rotors, which were coupled on the water surface via the camphor layer. In this setting, the rotors exhibit the phenomenon of synchronization [39,40], in which rotors behave in unison with a delay. Furthermore, we rationalize the experiments by simulating a set of dynamical equations which emulate the observed relaxation oscillations.

The manuscript is arranged in four main sections: Introduction (Sec. I), Experiments (Sec. II), Numerical Model (Sec. III), and Discussion and Summary (Sec. IV). Furthermore, Sec. II is divided into two subsections that describe (A) the experimental methods and preparation and (B) the results. Similarly, Sec. III is divided into two subsections describing (A) the numerical model and (B) the simulation results. Finally, the results are summarized and discussed in Sec. IV.

II. EXPERIMENTS

A. Method and preparation

The experiments were performed in a sliced inverted rectangular pyramid shaped glass container. This lower rectangle in this container had dimensions of 30 cm \times 20.5 cm and the upper rectangle had the dimension of 34.5 cm \times 25 cm. The depth of the container from the upper to the lower rectangle was 4.2 cm. To block air disturbances interfering with the rotors’ dynamics, the experiments were performed inside a plexiglass enclosure. Figure 1 shows the schematic diagram depicting the experimental setup’s side (left) and camera (right) view. The room temperature for all the experiments

was set between $25.2 \pm 0.7^\circ\text{C}$. The relative humidity lies between 49% and 69%.

To make pivot(s), thin needle(s) (red color in Fig. 1) was (were) fixed on a black painted aluminium sheet. For the third set of experiments, two needles were fixed at 6.0 cm and 4.2 cm distance, respectively. We placed an aluminium sheet fitted with pivots inside the glass container, which was later filled with 900 ml deionized water. With an aim of reducing the surface area exposed to rotor(s), we take a regular plastic sheet and cut a 11 cm \times 6 cm rectangular section in the middle. This plastic sheet was placed gently on a water surface such that the pivot was in the middle of the rectangular section.

Rectangular strips of dimensions 2.0 cm \times 0.4 cm were drawn on a computer and printed on a clean A4 size paper sheet with a black and white laserjet printer. The strips were kept black in color with a white circular dot at one end to aid with rotation tracking. At the other end of each paper strip, a hole was punched with a needle. 100 μl of 1.2M solution of laboratory-grade camphor in ethanol (purity 99.9%) was poured onto each ribbon. The strips were left in the poured solution for 60 s and then left to dry in the air for 600 s. After ethanol had dried off from the rectangular paper, only camphor was left on it. Throughout this manuscript, we will refer to this camphor infused paper as *camphor rotor ribbon*. Finally, these ribbons were pivoted on the thin needles and were introduced at the air-water interface through the holes. On touching the water surface, the camphor ribbon starts to rotate immediately. Initial environmental fluctuations decide the initial rotation direction, and hence it can be clockwise (cw) or counterclockwise (ccw) [31]. This ribbon continues its rotation in this initial direction unless externally perturbed.

The dynamics of ribbons were recorded with a high-speed video camera (GoPro Hero-4, frame rate 120 Hz, 720 p resolution), placed vertically above the glass container. The experimental videos were analyzed in MATLAB using the standard particle tracking code (adapted for MATLAB by Blair and Dufresne [41], which is based on the Crocker and Grier [42] algorithms). This algorithm returned x and y positions of the tracked white dots, which we refer to as the rotors’ positions. However, for visual convenience, we choose to show the speed time series of the rotors. Speed was calculated from the rotor’s x and y positions every 0.5 s (60 frames).

B. Results

This section is divided into two subsections, where the results are presented for a single rotor and two rotors. Furthermore, in the single rotor case, results are shown for both the autonomous as well as the entrained dynamics.

1. Single rotor

Autonomous. The word “autonomous” here refers to the natural dynamics of a single rotor. In this set of experiments, a single ribbon was placed at the water surface. Initially, the camphor ribbon showed periodic rotational motion, exhibiting regular oscillations. However, after some time has elapsed, the rotors start exhibiting an aperiodic rotational motion. In the current work, we discarded the initial periodic motion and focused on the aperiodic component of the rotors’ motion.

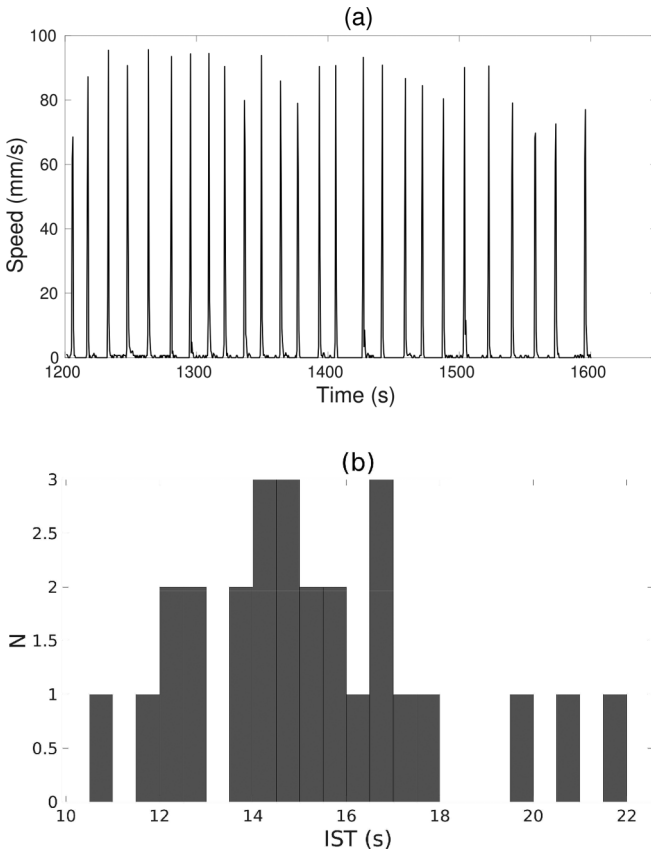


FIG. 2. Autonomous camphor rotor dynamics in the aperiodic regime. Panel (a) shows the temporal evolution of rotor speed. Panel (b) shows the corresponding histogram (bin count = 20; bin width = 0.5) of interspike interval time (IST). N denotes count of interspike interval time.

Figure 2(a) shows the temporal evolution of the rotors' speed between 1200 s and 1600 s (0 s was set when the ribbon touched the water surface). The salient feature of the rotors' dynamics is the bursting or spiking nature of its motion, wherein the rotor halts (almost zero speed) and then moves after irregular periods of time. This bursting is aperiodic and hence is characterized by irregular interspike intervals. We define an interspike interval as the time span between two successive speed maxima. In Fig. 2(b), a histogram provides evidence of a distributed interspike interval and hence a signature of aperiodicity or irregularity in the speed time series and the rotors' dynamics.

It should be emphasized that, after a halt, the camphor ribbon is stochastically triggered by environmental fluctuations, and it randomly rotates in either cw or ccw direction. Therefore, during each halt-move cycle, the rotor can switch its rotation direction (see Supplemental Material video s1.mp4 [43]).

Entrainment. Next, we seek control over these irregular rotor dynamics with external periodic forcing. A miniature dc air pump (CJP31-C03A1) was used for this purpose. This pump created a small but periodic air disturbance at the water surface. Previous work [44] has verified that the pump acts as a source of environmental perturbation, and not as a source of any significant kinetic energy to the system. The

air pump was clamped on a stand which was placed near the glass container. The position of the pump was such that its air-output nozzle pointed directly towards the pivot needle. A 1.5 V dc voltage supply powered the miniature pump. Furthermore, the on and off state of the pump was controlled by a periodic signal generated by a signal generator (Tektronix AFG-3022C). The signals' waveform was rectangular and its amplitude was +5 V. The pulse width of the periodic signal was kept constant at 0.5 s. Therefore, in each experimental run, the pump was ON for 0.5 s and OFF for $(T-0.5)$ s, wherein T represents the signals' time period. The ON state of the pump is indicated by a loud noise (see Supplemental Material video s2.mp4 [43]). For readers' visual convenience, we have manually written ON in the video whenever the pump is in the ON state. Furthermore, in Fig. 3(d) (inset), we have shown the time series of the pumps' state, i.e., the external forcing signal. The sound signal was extracted from the entrainment experiment video (s2.mp4) using standard MATLAB filters to plot this time series.

For this set of experiments, again, a fresh camphor ribbon was placed onto the water surface. In the aperiodic regime, we present results corresponding to the OFF-ON-OFF state of the forcing signal (Fig. 3). An OFF state here refers to the pump being completely switched off, whereas an ON state refers to the periodic switching of the pump as described above. The data in each state is plotted for 100 s. After the first OFF state [Figs. 3(a) and 3(b)], the forcing signal was switched ON for 100 s at 100 mHz frequency (time period = 10 s). We choose the pump switching frequency based on the rotors' autonomous frequency in the first OFF state. In the ON state of the pump, the rotor showed a remarkable response to an external forcing (see video s2.mp4). Whenever the pump is ON, the rotor moved either in cw or ccw direction. Figure 3(c) shows a spike in rotor speed every ≈ 10 s, hence corroborating the rotors' entrainment to the external forcing frequency. After the pump is switched OFF, the rotor returns to aperiodic dynamics [Figs. 3(e) and 3(f)]. A comparison of interspike interval histograms in OFF [Fig. 3(b)], ON [Fig. 3(d)], and OFF [Fig. 3(f)] shows that the forcing signal has squeezed the interspike interval distribution to around 10 s. Therefore, the pump has evoked nearly periodic dynamics at a predetermined frequency, in an otherwise aperiodically rotating camphor ribbon.

We want to point that, in the second OFF state, the interspike interval shifts towards higher values. This shift is not because of the air pump but the natural slowing down of the rotor with time. This slowdown is in agreement with previous observations reported in our other related works [31,32]. A possible cause of this slowdown is discussed in Sec. III. Furthermore, this continuous decay in the autonomous frequency of the rotor restricted its entrainment for a long time.

2. Two rotors

To investigate the collective behavior of aperiodic rotors, two rotors were now placed at the water surface. The rotors were kept at a pivot to pivot distance (l) greater than l_c . We define l_c as twice the length of a single ribbon (2×2.0 cm = 4.0 cm). It should be noted that, at $l > l_c$, rotors do not physically collide. Figure 4 depicts the irregular dynamics of

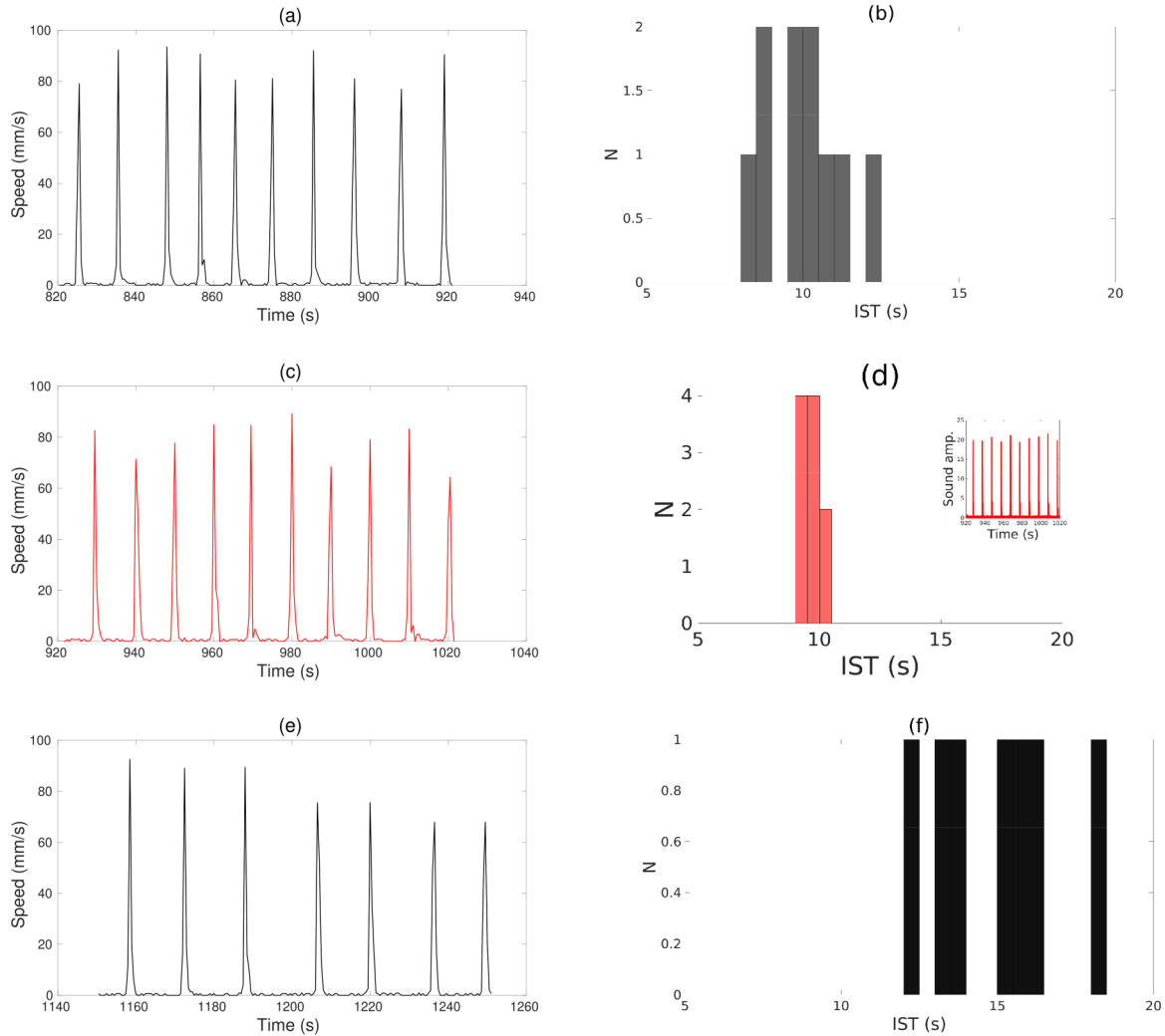


FIG. 3. Entrainment: time series of speed (a),(c),(e) and histogram (b),(d),(f) of interspike time interval (IST) for OFF-ON-OFF pump state. N denotes the count of interspike interval. Bin count = 20; bin width = 0.5 for histograms. Panels (a),(b) and (e),(f) show aperiodic dynamics of the camphor rotor before the pump was turned ON and after the pump was turned OFF. Red plots (c),(d) show the speed and histogram of the interspike interval when the pump is ON. Both plots portray nearly periodic dynamics characterized as a constant interspike time interval. The inset inside panel (d) shows the pump (forcing) status. A high sound amplitude corresponds to the ON state of the pump, while zero sound amplitude corresponds to the OFF state.

a coupled rotors pair. We placed two camphor rotors at a pivot to pivot distance $l = 4.2$ cm. After the transient dynamics have elapsed, both the rotors were found to exhibit irregular dynamics at the air-water interface. Figure 4 shows the speed time series of both rotors from 1300 s–1500 s (0 s is when the first rotor touched the water surface). It is clear that when one rotor burst into motion, the other one follows its burst almost instantaneously or with a time delay (see Supplemental Material video s3.mp4). Nonetheless, both rotors respond to each other’s movement and perform synchronized bursting on the water surface. Rotors are coupled through the exchange of camphor molecules at a common fluid surface. This type of indirect chemical coupling between camphor particles has been reported previously in [31,45]. As previously mentioned, in the irregular domain, rotors are in a stochastically triggered intermittent state. Therefore, we believe that a random burst in one of the rotors acts as an environmental fluctuation and triggers the motion in the other rotor.

III. SIMULATIONS

In this section, we will discuss the numerical model and simulation results.

A. Model

To corroborate our experimental observations, we carried out simulations incorporating a three-dimensional excitable system. To reiterate, a rotor shows bursting dynamics and, after each halt, it can burst in cw or ccw direction. Inspired by this, in numerics, we choose a quintic nullcline system [Eqs. (1)–(3)], such that the angular speed is kept at an excitable fixed point. Furthermore, we intuit that noisy environmental fluctuations generate bursts in rotor dynamics. Therefore, a fixed amplitude noise [Eq. (3)] was used to trigger excitable oscillations in the system. The quintic term in the temporal evolution of angular speed ensures that noise can

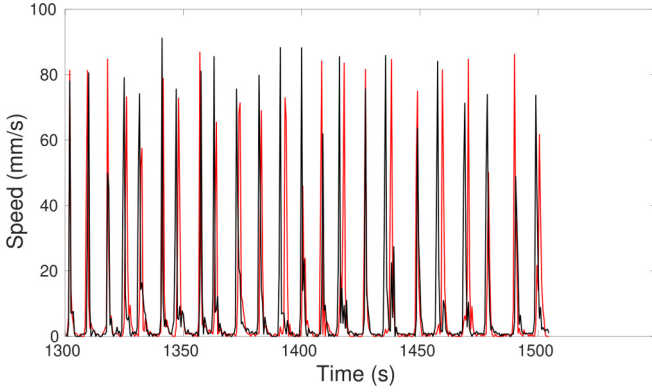


FIG. 4. Speed time series of two coupled aperiodic camphor rotors. Red and black curves correspond to first and second camphor rotor.

randomly kick angular speed in a positive (cw) or negative (ccw) direction. Denoting the angular displacement, speed, and acceleration as θ , ω , and α , respectively, the dynamical equations are as follows:

$$\dot{\theta}(t) = \omega(t), \quad (1)$$

$$\dot{\omega}(t) = \epsilon[-\omega^5(t) + 2\omega^3(t) - \omega(t) - \alpha(t)], \quad (2)$$

$$\dot{\alpha}(t) = \omega(t) + D\eta(t), \quad (3)$$

wherein $\eta(t)$ is a Gaussian white noise centered around zero and having unit variance and D refers to the noise strength. For $D = 0$, fixed point $(0,0,0)$ is a stable fixed point; hence the system will not show bursting dynamics if unperturbed. Subsequently, to mimic entrainment in numerical settings, we added a periodic external perturbation in Eq. (3) as follows:

$$\dot{\alpha}(t) = \omega(t) + As(t) + D\eta(t), \quad (4)$$

where A is the amplitude of periodic rectangular pulses $s(t)$. These pulses correspond to periodic switching ON and OFF of the miniature air pump in experiments.

Lastly, we studied two coupled excitable systems [Eqs. (1)–(3)] respective to the third set of experiments (Sec. B 2). As mentioned previously, a burst in one of the rotors seems to activate the burst in the other rotor. We believe that, for synchronized bursting, the angular speed of rotors should mutually adjust, and the term responsible for coupling will be angular speed [Eqs. (5)–(7)]. Imagine the coupling as if camphor concentration around one rotor is transported to the other rotor. For $i, j = 1, 2$, the equations are as follows:

$$\dot{\theta}_i(t) = \omega_i(t), \quad (5)$$

$$\dot{\omega}_i(t) = \epsilon[-\omega_i^5(t) + 2\omega_i^3(t) - \omega_i(t) - \alpha_i(t)], \quad (6)$$

$$\dot{\alpha}_i(t) = \omega_i(t) + D\eta(t) + K\omega_j. \quad (7)$$

The parameter K in Eq. (7) corresponds to the magnitude of perturbation experienced by a rotor due to the motion of the other. It incorporates the combined effect of the pivot to pivot distance between the two rotors and the chemical coupling due to shared camphor concentration fields.

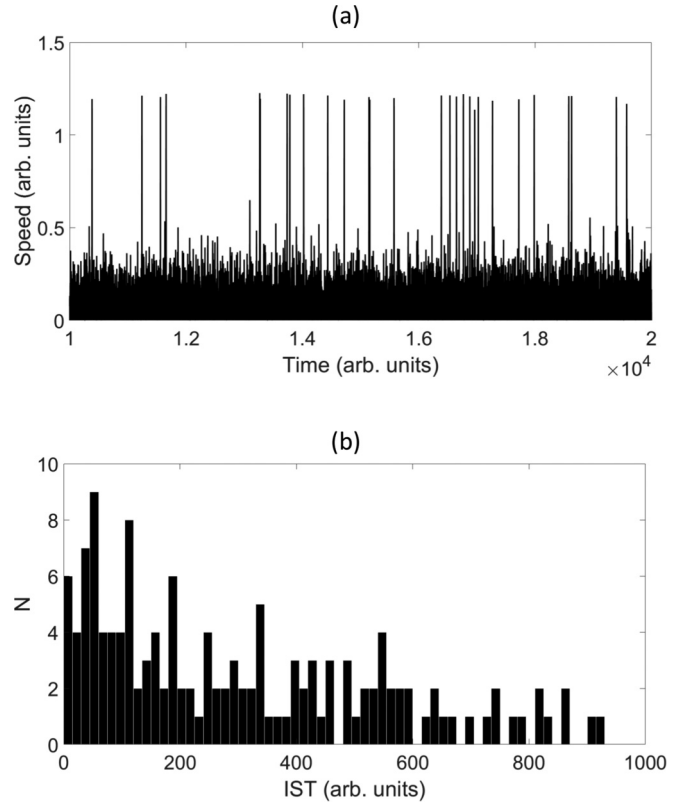


FIG. 5. Numerical results for the autonomous oscillator. (a) The temporal evolution of speed; panel (b) shows the corresponding histogram of the interspike interval time (IST). N denotes the count of interspike interval.

B. Results

This aforementioned set of equations was simulated using a Runge-Kutta fourth order algorithm with a time step of 10^{-3} . The first 1000 time units (1 time unit = 10^3 time steps) were discarded as transients and data was analyzed for the next 49 000 time units. In Figs. 5, 6, and 7 a considerable portion of the analyzed data is presented. For all numerical cases, the noise amplitude D and ϵ was set to be 0.5 units and 50 units, respectively. Initial values of ω and α were kept fixed at 0.0 unit and 0.01 unit, respectively. The initial value of θ , on the other hand, was chosen randomly in the range $[0, 2\pi]$. In the following subsections, we will talk about detailed simulation results corresponding to the three sets of experiments.

1. Single oscillator

Autonomous. Figure 5 shows the (a) temporal evolution of angular speed and (b) distribution of the interspike interval for autonomous differential equations (1)–(3).

The time series shows large spikes in the angular speed aperiodically occurring on top of a bed of noisy fluctuations. Consequently, the histogram of interspike intervals exhibits a broad range distribution. Both Figs. 5(a) and 5(b) confirm the aperiodic nature of the bursting dynamics.

Entrainment. In this case, Eqs. (1), (2), and (4) were simulated with the amplitude of the periodic signal (A) being fixed at 0.2. The signal was high (ON) for $0.01T$ time units and zero (OFF) for the remaining time period, i.e., $T - 0.01T$

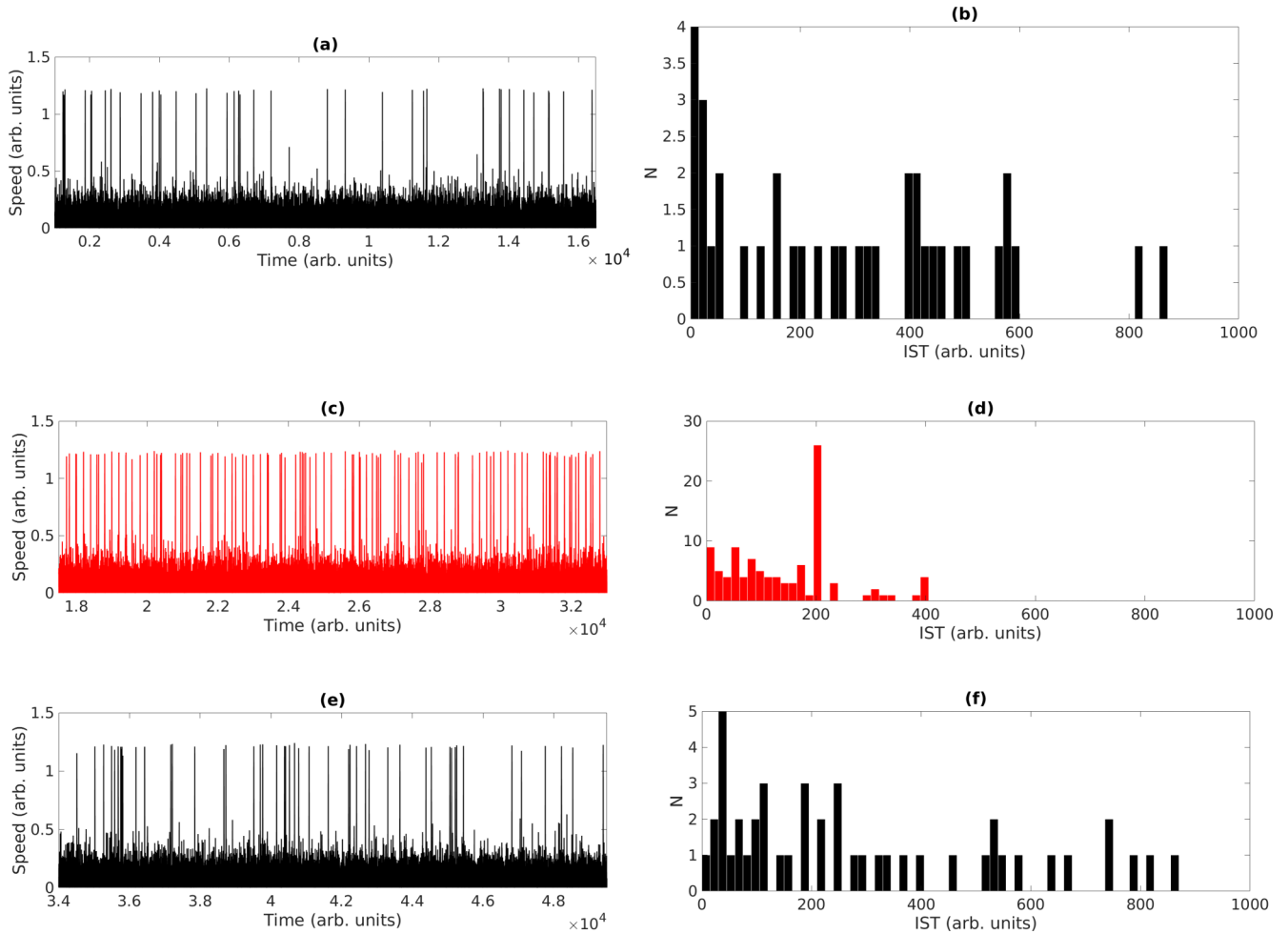


FIG. 6. Entrainment: numerical time series of speed (a),(c),(e) and histogram (b),(d),(f) of interspike time interval (IST) for OFF-ON-OFF periodic signal. N denotes the count of interspike interval. Panels (a),(b) and (e),(f) show aperiodic dynamics before switching ON external forcing and after the forcing was OFF. Red plots (c),(d) show speed and histogram of the interspike interval when the periodic signal was ON.

time units. T here stands for 200 time units. Following the same procedure as done experimentally, in Fig. 6, we have presented the speed time series and the interspike interval for the OFF-ON-OFF state. When there is no external signal (OFF state), the dynamics is irregular and the same is evident from Figs. 6(a), 6(b) and Figs. 6(e), 6(f). However, in the presence of external forcing (ON state), a relative control over aperiodic dynamics was observed [Figs. 6(c) and 6(d)]. When compared to the OFF state, the bursting in the ON state is relatively regular. The width of the interspike interval distribution has reduced and is found to be centered around the external signal's time period (200 time units).

2. Two oscillators

Figure 7 reports the simulation results corresponding to dynamical equations (5)–(7). Angular speeds' temporal evolution for the two-oscillator system is presented for (a) coupling OFF state ($K = 0.0$ unit) and (b) coupling ON state ($K = 0.7$ unit). It is evident from Fig. 7(b) that, when coupled, both the oscillators fire nearly simultaneously.

IV. DISCUSSION AND SUMMARY

In this work, we reported aperiodic dynamics, control of aperiodicity, and synchronized bursting of camphor rotors. A camphor rotor, when placed on an air-water interface, forms a camphor layer on the water surface. Any environmental fluctuations at this point may lead to the anisotropic distribution of the camphor layer. This inhomogeneously distributed layer results in a net surface tension gradient around the rotor, and hence a Marangoni force in the higher surface tension direction. Initial rotation direction can be cw or ccw and is picked up randomly. Once the ribbon starts rotating in a particular direction, this motion of the rotor itself maintains an asymmetry in camphor concentration. Thus the ribbon would continue rotating until disturbed externally or the surface activity is diminished.

After some transient dynamics, this rotor enters into an aperiodic bursting regime, wherein it performs irregular rotations. Furthermore, the rotor showed intermittent bursting characterized as irregular spikes in speed. A spread in the speed interspike interval distribution confirmed this aperiodic nature of the rotor dynamics. In the surface area available to the ribbon, we believe that, as time progresses, the camphor

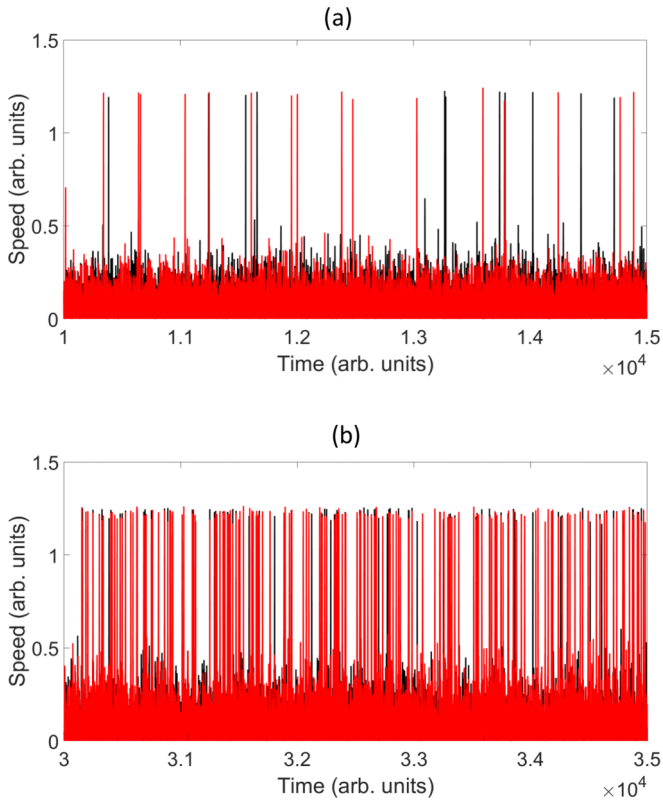


FIG. 7. Numerical speed time series of (a) two uncoupled aperiodic oscillators ($K = 0.0$ unit) and (b) two coupled aperiodic oscillators ($K = 0.7$ unit). In (b), the red and the black curves correspond to the first and the second oscillator, respectively.

layer globally reduces the surface tension. This causes the ribbon to enter a metastable excitable state. In this state, any minute environmental fluctuation can trigger activity in the rotor. We would like to emphasize here again that the camphor rotor has a finite life span on the water surface. We argue the rotors' finite life is due to the accumulation of camphor

molecules on the surface of water coupled with loss of the rotors' fuel, i.e., camphor [33]. These two factors together result in lowering the surface tension gradient at the air-water interface. Hence less Marangoni driving forces act on the rotor.

Following this characterization, we showed that the control of this aperiodicity in rotor dynamics could be achieved with external enforcement. A miniature air pump acts as a periodic environmental perturbation on the water surface and gives rise to periodic rotations of ribbon. We subsequently conducted experiments on two coupled aperiodic rotors and reported synchronized bursting of these rotors. The camphor layer around one rotor interacts with the camphor layer of the other rotor and results in a chemical coupling.

To probe further into such excitable dynamics and gain a better understanding of the phenomenon underlying our experimental observations, we presented a numerical model incorporating excitable differential equations. The model was able to qualitatively reproduce the experimental observation for one and two aperiodic rotors. We believe that our tabletop experiments, showing aperiodic bursting dynamics of the active rotor, are an exciting contribution showing the nonlinear aspects related to the active matter field. Our experiments showing the control of aperiodic self-rotations of camphor ribbon on the air-water surface might inspire researchers to investigate similar behavior in other self-propelled particles. Our model was able to demonstrate that the mechanism behind the experimental observations can be explained by a rudimentary excitable system without using complex fluid dynamical equations. Our approach of modeling the experiments via a general model makes the insights from it more widely applicable in a plethora of nonlinear systems.

ACKNOWLEDGMENTS

We have benefited from the discussions with NLD laboratory members at IIT Bombay. J.S. would like to thank MHRD (India), IRCC and Department of Physics, IITB (India) for financial support. I.T. acknowledges financial support from CSIR (India).

- [1] A. Pikovsky, M. Rosenblum, and J. Kurths, *Synchronization: A Universal Concept in Nonlinear Sciences* (Cambridge University Press, Cambridge, UK, 2003), Vol. 12.
- [2] J. S. Fein and R. L. Pfeffer, *J. Fluid Mech.* **75**, 81 (1976).
- [3] B. Dennis, R. Deshmairis, J. Cushing, and R. Costantino, *J. Anim. Ecol.* **66**, 704 (1997).
- [4] P. Parmananda, G. J. E. Santos, M. Rivera, and K. Showalter, *Phys. Rev. E* **71**, 031110 (2005).
- [5] T. R. Chigwada, P. Parmananda, and K. Showalter, *Phys. Rev. Lett.* **96**, 244101 (2006).
- [6] P. Parmananda, H. Mahara, T. Amemiya, and T. Yamaguchi, *Phys. Rev. Lett.* **87**, 238302 (2001).
- [7] B. Robert, F. Alin, and C. Goeldel, in *ISIE 2001. 2001 IEEE International Symposium on Industrial Electronics Proceedings (Cat. No. 01TH8570)* (IEEE, New York, 2001), Vol. 3, pp. 2136–2141.
- [8] D. Harter and R. Kozma, *Int. J. Intell. Syst.* **21**, 955 (2006).
- [9] S. L. Kingston and K. Thamilaran, *Int. J. Bifurcation Chaos* **27**, 1730025 (2017).
- [10] A. L. Hodgkin and A. F. Huxley, *Proc. R. Soc. London, Ser. B* **140**, 177 (1952).
- [11] Y. Yu, W. Wang, J. Wang, and F. Liu, *Phys. Rev. E* **63**, 021907 (2001).
- [12] E. Allaria, F. T. Arecchi, A. Di Garbo, and R. Meucci, *Phys. Rev. Lett.* **86**, 791 (2001).
- [13] A. Garfinkel, M. L. Spano, W. L. Ditto, and J. N. Weiss, *Science* **257**, 1230 (1992).
- [14] S. J. Schiff, K. Jerger, D. H. Duong, T. Chang, M. L. Spano, and W. L. Ditto, *Nature (London)* **370**, 615 (1994).
- [15] P. Kumar and P. Parmananda, *Chaos: Interdiscip. J. Nonlinear Sci.* **28**, 045105 (2018).

- [16] P. Kumar, P. Parmananda, D. K. Verma, T. Singla, I. de Nicolás, J. Escalona, and M. Rivera, *Chaos: Interdiscip. J. Nonlinear Sci.* **29**, 053112 (2019).
- [17] R. Phogat and P. Parmananda, *Chaos: Interdiscip. J. Nonlinear Sci.* **28**, 121105 (2018).
- [18] J. M. Cruz, A. Hernandez-Gomez, and P. Parmananda, *Phys. Rev. E* **75**, 055202(R) (2007).
- [19] E. Schöll and H. G. Schuster, *Handbook of Chaos Control, Second Edition* (Wiley-VCH Verlag GmbH & Co. KGaA, 2007).
- [20] M. Nagayama, S. Nakata, Y. Doi, and Y. Hayashima, *Physica D* **194**, 151 (2004).
- [21] S. Nakata, V. Pimienta, I. Lagzi, H. Kitahata, and N. J. Suematsu, *Self-Organized Motion: Physicochemical Design Based on Nonlinear Dynamics* (Royal Society of Chemistry, London, 2018).
- [22] A. Vilk, I. Legchenkova, M. Frenkel, and E. Bormashenko, *Condens. Matter* **5**, 51 (2020).
- [23] S. Nakata and Y. Hayashima, *J. Chem. Soc., Faraday Trans.* **94**, 3655 (1998).
- [24] S. Soh, M. Branicki, and B. A. Grzybowski, *J. Phys. Chem. Lett.* **2**, 770 (2011).
- [25] C. Tomlinson, *London, Edinburgh, Dublin Philos. Mag. J. Sci.* **38**, 409 (1869).
- [26] S. Nakata, M. Nagayama, H. Kitahata, N. J. Suematsu, and T. Hasegawa, *Phys. Chem. Chem. Phys.* **17**, 10326 (2015).
- [27] A. Biswas, J. Cruz, P. Parmananda, and D. Das, *Soft Matter* **16**, 6138 (2020).
- [28] I. Tiwari, P. Parmananda, and R. Chelakkot, *Soft Matter* **16**, 10334 (2020).
- [29] M. Frenkel, A. Vilk, I. Legchenkova, S. Shoval, and E. Bormashenko, *ACS omega* **4**, 15265 (2019).
- [30] J. Gorecki, H. Kitahata, Y. Koyano, M. Gryciuk, M. Malecki, and N. J. Suematsu, *Int. J. Unconv. Comput.* **13**, 417 (2017).
- [31] J. Sharma, I. Tiwari, D. Das, P. Parmananda, V. S. Akella, and V. Pimienta, *Phys. Rev. E* **99**, 012204 (2019).
- [32] J. Sharma, I. Tiwari, D. Das, V. Pimienta, and P. Parmananda, *Phys. Rev. E* **101**, 052202 (2020).
- [33] J. Sharma, I. Tiwari, D. Das, and P. Parmananda, *Phys. Rev. E* **103**, 012214 (2021).
- [34] S. Nakata and S.-i. Hiromatsu, *Colloids Surf., A* **224**, 157 (2003).
- [35] N. J. Suematsu, K. Tateno, S. Nakata, and H. Nishimori, *J. Phys. Soc. Jpn.* **84**, 034802 (2015).
- [36] Y. Hayashima, M. Nagayama, Y. Doi, S. Nakata, M. Kimura, and M. Iida, *Phys. Chem. Chem. Phys.* **4**, 1386 (2002).
- [37] V. Akella, D. K. Singh, S. Mandre, and M. Bandi, *Phys. Lett. A* **382**, 1176 (2018).
- [38] N. J. Suematsu, Y. Ikura, M. Nagayama, H. Kitahata, N. Kawagishi, M. Murakami, and S. Nakata, *J. Phys. Chem. C* **114**, 9876 (2010).
- [39] D. K. Verma, H. Singh, A. Contractor, and P. Parmananda, *J. Phys. Chem. A* **118**, 4647 (2014).
- [40] D. K. Verma, H. Singh, P. Parmananda, A. Contractor, and M. Rivera, *Chaos: Interdiscip. J. Nonlinear Sci.* **25**, 064609 (2015).
- [41] D. Blair and E. Dufresne, Particle-tracking code available at <http://physics.georgetown.edu/matlab>.
- [42] J. C. Crocker and D. G. Grier, *J. Colloid Interface Sci.* **179**, 298 (1996)..
- [43] See Supplemental Material at <http://link.aps.org/supplemental/10.1103/PhysRevE.105.014216> for Single autonomous aperiodic camphor rotor moving at the surface of the water (video s1.mp4), single entrained camphor rotor (video s2.mp4) and two synchronized aperiodic camphor rotors (video s3.mp4). Sound in s2.mp4 corresponds to the ON state of the mini air pump.
- [44] I. Tiwari, S. Upadhye, V. Akella, and P. Parmananda, *Soft Matter* **17**, 2865 (2021).
- [45] N. J. Suematsu, S. Nakata, A. Awazu, and H. Nishimori, *Phys. Rev. E* **81**, 056210 (2010).